Aspects of Network Formation in Glassy Thermosets

Andrew T. Detwiler, Alan J. Lesser

Department of Polymer Science and Engineering, University of Massachusetts Amherst, Amherst, Massachusetts 01003

Received 17 July 2009; accepted 29 October 2009
DOI 10.1002/app.31681
Published online 26 March 2010 in Wiley InterScience (www.interscience.wiley.com).

ABSTRACT: Aspects of network formation and the physical properties of stoichiometric amine-cured epoxy resins are investigated. The state of network formation is systematically controlled by using isothermal cure conditions and a linear temperature ramp condition. Affine deformation in compression at a constant true strain rate is used to measure the true stress–strain response from small strains to large strains. Beginning with the low-strain responses and continuing through yielding, partially cured samples demonstrate characteristics of physical ageing that diminish as the networks approach full conversion. The postyield properties are characterized by a strong dependence on network connectivity with little influence of the curing method. The mechanical responses are also applied to necking and shear banding analyses. The resins are unable to achieve stable necking in tension. However, shear bands are able to be stabilized, as predicted by a model developed in this work. These results suggest that physical ageing is inherent in epoxy network formation, and the resulting strain localization significantly degrades the mechanical integrity of epoxy resins in the partially cured state, regardless of the cure conditions. © 2010 Wiley Periodicals, Inc. J Appl Polym Sci 117: 1021–1034, 2010

Key words: necking; mechanical properties; networks; structure–property relationships; thermosets

INTRODUCTION

Physical ageing has been widely studied in thermoplastic systems where it has been associated with increases in density, modulus, and yield stress and with changes in other rate- and temperature-dependent properties.[1–3] The underlying physical consequences of the submolecular relaxations associated with physical ageing are increases in relaxation times and decreases in free volume. From an engineering perspective, it is important to know the thermal and mechanical history of a material to be able to predict physical and mechanical properties over its lifetime. McKenna has shown with polycarbonate that mechanical and thermal rejuvenation do not produce identical states, and the yield stress evolves to different equilibrium values depending on the type of rejuvenation.[4] However, Govaert and coworkers showed mechanical rejuvenation and thermal treatments of polycarbonate only differed with respect to the "age" of the resulting material.[5]

Thermoplastics have received much of the attention from researchers in the physical ageing literature due to their widespread application and somewhat more straightforward characterization relative to that of thermosets. Far less work has been reported on the effects of physical ageing in thermosets. Particularly in densely crosslinked systems where the relaxation of highly constrained chain segments into denser, less flexible conformations may be significantly hindered by the topological connections of the networks. Some authors who have studied physical ageing in glassy thermosets have seen responses similar to those observed in thermoplastics.[6–9] A fundamental difference between most thermoplastics and thermosets is the processing conditions involved in their manufacture. Commercial thermoplastics are generally polymerized and pelletized before being shipped to a processing plant where they undergo some sort of molding operation. In contrast, thermosets such as epoxies, polyurethanes, and phenolics become intractable when they are polymerized. As a result, the monomers or precursors must be molded into their final form before they are fully cured. This intractability also means the topological arrangement of chain segments and crosslinks is fixed during the reactive step of processing.

Initial studies by this research group on thermosets indicate that characteristics commonly observed in the physical ageing of thermoplastics also occur in the early stages of epoxy network formation.[10] To further our understanding, and to compare partially cured model epoxy networks with the literature on network formation and physical ageing, a sensitive probe of network formation is needed. Differential

Correspondence to: A. J. Lesser (ajl@polysci.umass.edu).
Contract grant sponsors: Center for University of Massachusetts Industrial Research on Polymers, National Science Foundation Materials Research Science and Engineering Center.

scanning calorimetry (DSC) is one technique that allows the characterization of the thermal properties of epoxy networks, namely T_g and conversion. As a complimentary technique a number of authors have studied the small-strain and yield responses of various epoxy networks as a function of temperature and/or composition.[8,11–15] Relatively little work has considered the large-strain responses of glassy thermosets,[16,17] particularly in the strain-hardening regime.

Lesser and Calzia used simple compression to test the strain-hardening properties of a series of fully cured networks with systematically varied molecular weight between crosslinks (M_c).[18] In their work, M_c was controlled by stoichiometrically varying the ratio of a difunctional amine chain extender to a tetrafunctional amine crosslinker. They found the strain-hardening moduli of model aliphatic (more flexible backbone) and aromatic (stiffer backbone) epoxy resins to be highly correlated with M_c. By studying flexible aliphatic as well as stiffer aromatic crosslinkers and chain extenders, they were able to show that the strain hardening response is independent of backbone stiffness. However, they also found that G_R decreases with increasing temperature in the glassy state. This temperature dependence suggests strain hardening is not a purely entropic process in the glassy state.

In this study, we use compression and other physical characterization techniques to analyze glassy network formation during the curing process. Physical and mechanical data are compared using several physical models. In addition, a model is developed to predict strain localization behavior as it applies to necking and shear banding. The purpose of the current work is not to investigate physical ageing or methods of rejuvenation, however, comments are made with regard to the effect of thermal treatments and mechanical deformation on the materials investigated herein.

METHOD

Stoichiometric mixtures of difunctional epoxide resin based on a purified diglycidyl ether of bisphenol A (DGEBA; DER 332, epoxide equivalent weight 175 g/mol); difunctional *N,N′*-dimethylethylenedianime (DMEDA Aldrich 90+%); and tetrafunctional ethylenediamine (EDA Aldrich 99+%) were poured into cylindrical glass molds treated with a release agent. The molds were placed in a 23°C water bath for several hours to control the exothermic reaction.

For an isothermal cure condition, the molds were transferred from the water bath to nitrogen gas purged ovens at the desired cure temperatures (between 23°C and 165°C). Samples were cured isothermally for 18 h to maximize the level of conversion possible at that temperature.

For a ramped cure condition, molds were transferred from the water bath to an oil bath at 25°C. The oil bath was then heated at a rate of 40°C per hour to 165°C. At intermediate temperatures molds were removed and quenched to room temperature in water baths to give partially cured samples. Samples were stored in a freezer at −10°C to prevent further curing and to inhibit physical ageing until they could be tested. Some partially cured samples from both the isothermal and ramp series were also postcured at 165°C for 4 h to observe the effect of cure path on their properties in the fully cured state.

The T_g of each resin was determined as the inflection point of the heat flow versus temperature curve from DSC heating at 10°C per minute in a TA Instruments DSC 2910. Conversion was measured as the integration of the exotherm in the dH/dT curve of each resin.

Compression bullets were formed by cutting the cylinders into sections with height to diameter ratios of 1:1. Care was taken to machine the top and bottom faces of the cylinders such that they were parallel to each other and perpendicular to the sides of the cylinders. The faces were polished to give smooth, glassy surfaces. Density was measured at 23°C by the water displacement method (ASTM D792). Dimensions for compression testing were measured to the nearest 0.01 mm using calipers.

Immediately before compression testing a surfactant-PTFE film-surfactant treatment was applied to the top and bottom surfaces of the compression specimens to produce a low friction surface, which would allow for affine deformation over a large range of strains. The samples were loaded in compression using an Instron 5800 fitted with a 50 kN load cell and controlled using the Merlin software package. Samples were tested at 20°C and a constant true strain rate of 0.1 mm/mm/min (1.67×10^{-3} s^{-1}) was maintained during the entire test.

Tensile testing was conducted on ASTM D638 Type I samples machined from 3-mm thick plaques. Samples were tested at 20°C using a strain rate of 1.67×10^{-3} s^{-1} on the same instrument described for compression testing (see above).

Characterization of shear bands was achieved by compressing rectangular specimens containing precracks intended to promote shear. Rectangular samples with dimensions of $40 \times 13 \times 6$ mm^3 were tested in compression in a modified IITRI fixture (see Fig. 8), which prevents buckling while allowing shear bands to be photographed *in situ* through the hole. The samples are placed upright between the two aluminum plates and the screws are hand tightened. Before testing fresh razor blades are tapped into 6 mm slots cut into the samples at 45° to

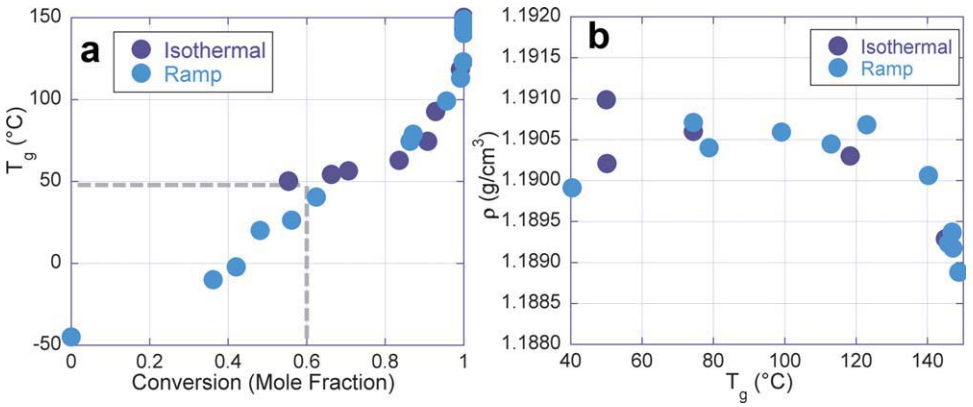

Figure 1 (a) T_g as a function of conversion. Dashed lines indicate critical conversion and critical T_g. (b) Density as a function of T_g.[Color figure can be viewed in the online issue, which is available at www.interscience.wiley.com.]

promote shear band formation. A series of lines oriented perpendicular to the precracks are scratched into the sample surface to measure shear optically.

DISCUSSION

T_g-conversion

The T_g of an epoxy resin increases as the conversion increases and the two have been shown to be well correlated.[11,14,19,20] Differential scanning calorimetry (DSC) is widely used to measure T_g and conversion. T_g is often measured as the inflection point of the step change in the heat release rate versus temperature curve. Conversion (x) is calculated by integrating under the heat of reaction peak (ΔH) above T_g in a plot of heat release rate (normalized by sample mass) versus temperature, then dividing by the heat of reaction of an uncured sample (ΔH_0) according to eq. (1).[21]

$$x = 1 - {}^{\Delta H}/_{\Delta H_0}, \tag{1}$$

DGEBA is a difunctional epoxide and EDA is a tetrafunctional amine. When fully cured these monomers form a model network consisting of tetrafunctional crosslinks.[6,22] However, at intermediate stages of cure the networks are less well defined as there is a distribution of EDA molecules that have reacted with zero, one, two, three, or four epoxide groups.[13,19,20,23] For our case, Flory's equation [eq. (2)] predicts the gel point to be at a critical conversion (x_c) of about 0.58.[24,25]

$$x_c = \frac{1}{[1 + (f - 2)]^{1/2}}, \tag{2}$$

where f is the average functionality or average number of labile amine hydrogen on each crosslinker molecule. This prediction assumes equal reactivity of all species with no side reactions, such as etherification of the epoxide groups with hydroxyl groups. Several groups have demonstrated epoxies with gel points in the vicinity of this prediction, although the values are always slightly higher than 0.58 due to intramolecular reactions.[24–26] At the critical conversion, the resins treated here transition from sol glasses to gel glasses. Accordingly, many of the physical and mechanical properties reported in this work demonstrate qualitative changes in behavior when conversion approaches the critical conversion.

Figure 1(a) shows T_g as a function of conversion for resins cured by the isothermal and ramped cure schedules. The nonlinear relationship between T_g and conversion has been reported by many authors using DSC[21] as well as FTIR absorbance to calculate conversion.[20,27] The data points from the two curing methods overlap, which suggests the T_g-conversion relationship is not sensitive to the curing method. This cure path insensitivity was also suggested by Wang and Gillham for a series of aromatic amine-cured epoxy resins.[19] It is notable that T_g increases sharply as the conversion approaches 1. As measures of conversion (from DSC or FTIR) are less sensitive than T_g to changes in the network in the high conversion regime, T_g is used throughout this paper as the quantitative measure of cure state.

Density

The monomers used to prepare these model epoxy networks begin as liquids at room temperature. The DGEBA has a density of 1.16 g/cm^3 while the EDA has a density of 0.899 g/cm^3. Density at 23°C is plotted as a function of T_g for the two series of partially cured resins [Fig. 1(b)]. Beyond the gel point, the resins have density values around 1.1905 g/cm^3. When they achieve maximum T_g, their density decreases slightly to $\sim$ 1.1890 g/cm^3, a decrease of 0.1%. Density evolves in a nonlinear manner in this system.

However, the changes in density are fairly small in this conversion range, especially when the precision of the measurements averages about ±0.0005 g/cm^3. The nonlinear evolution of density as a function of T_g and the effects of thermal history have been reported for other epoxy systems.[13,28–30] Density typically remains approximately constant from the gel point until resins approach the maximum T_g where density suddenly decreases. This decrease in density has been attributed to the lower coefficient of thermal expansion of polymers in the glassy region relative to that in the rubbery region. It is unlikely to be a result of further conversion since, although there is a significant change in T_g over this range (120–145°C), conversion is essentially complete [Fig. 1(a)]. This densification at maximum T_g is observed for all fully cured resins, including those initially cured at 165°C and those subjected to a postcure.

Below is a simplified diagram that qualitatively illustrates how the density of a typical epoxy resin changes during two different isothermal cure conditions[31] (Fig. 2). Path ABCDE depicts an isothermal cure where the cure temperature (T_c) is above the maximum T_g ($T_{g,\max}$) of the fully cured resin, whereas T_c' for path A′B′C′D′E′ is below $T_{g,\max}$. In ABCDE, the epoxide and amine monomers are heated from A to B, i.e., room temperature (T_0) to T_c. The density decreases during this process due to thermal expansion in the liquid state. From B to C, the system is held isothermally at T_c for some amount of time to allow the chemical reaction to proceed. There is isothermal shrinkage due to the curing reaction. The T_g of the system increases during this step due to the increase in molecular weight and the crosslinking reactions. When the system arrives at C, it is assumed that the resin is fully cured and no further chemical reactions take place. The resin is cooled in the rubbery state under quasi-equilibrium conditions from C until it approaches its T_g at D. The cooling continues from D to E in the glassy state under nonequilibrium conditions.

The other cure path, A′B′C′D′E′, uses a lower T_c' which produces a resin with lower T_g' and slightly higher density. Vitrification occurs during cure, as T_g' increases above T_c'. Therefore, points C′ and D′ overlap, and all cooling occurs in the glassy state. This cure path is typical of what partially cured epoxy resins experience as T_g tends to be between 10°C and 30°C greater than T_c, assuming the resin is reactive at T_c.[14,29,32,33]

There are several explanations put forward in the literature to explain the observed behavior in terms of chemical and physical changes, respectively, that occur during epoxy processing. The following two paragraphs treat the portions of Figure 2 that include the segments from B to C (chemical) and C to E (physical), respectively.

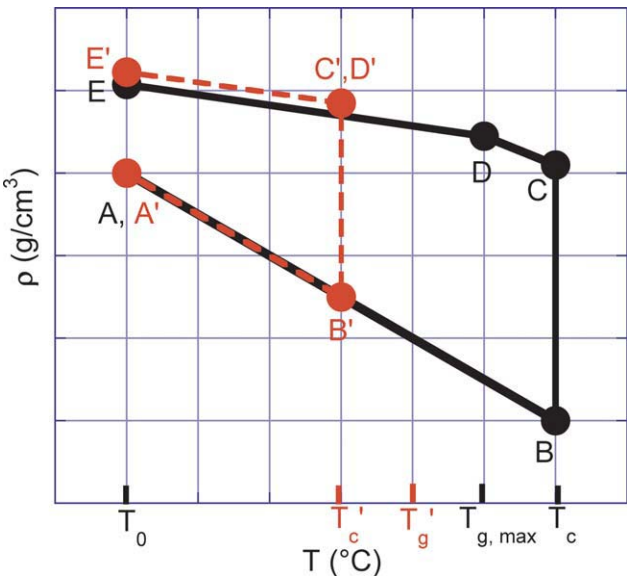

Figure 2 Density evolution during cure for two isothermal cure temperatures. For ABCDE $T_c > T_{g,\max}$. For A′B′C′D′E′ $Tc' < T_g'$. The prime symbols (′) are used to distinguish between the two paths. [Color figure can be viewed in the online issue, which is available at www.interscience.wiley.com.]

The volume occupied by a chain segment can be broken down into vibrational volume, van der Waals volume, and free volume.[34] Vibrational volume is assumed to be constant for an epoxy in the glassy state, independent of conversion.[34,35] On the basis of an analysis of the van der Waals contributions to volume over the course of curing a similar DGEBA-based epoxy system, others have shown that the van der Waals radius actually increases as epoxies cure.[35] This expansion was mainly attributed to the opening of the highly strained epoxide ring. However, positron annihilation studies have shown that free volume passes through a minimum in the vicinity of the gel point, followed by a small increase as cure procedes beyond the gel point in epoxy systems.[35] The reduction in free volume dominates over the van der Waals expansion effect until the gel point is reached, at which point free volume remains relatively constant while van der Waals based expansion continues until the resin is fully cured. In agreement with the literature, we observe a maximum in the room temperature density in the vicinity of the gel point and a decrease in density with further conversion.

If density is measured at room temperature it is necessary to cool the sample from an elevated cure temperature (T_c) to the measurement temperature. This consists in cooling in the rubbery state if $T > T_g$ and/or cooling in the glassy state when $T < T_g$. Molecular rearrangements in the rubbery state occur rapidly, thus equilibrium is reached in a matter of seconds.[34] However, molecular rearrangements in

the glassy state are orders of magnitude slower than in the rubbery state. Therefore, a material in the glassy state is unable to completely equilibrate when it is subjected to a finite cooling rate. This departure from equilibrium is evidenced by excess enthalpy (ΔH°), entropy (ΔS°), free energy (ΔG°), and volume (ΔV°). These excess quantities spontaneously decrease toward their equilibrium values, hence physical ageing.[2,36,37] However, the time scale of this equilibration is often longer than the experimental time scale, particularly when the difference between the measurement temperature and the T_g is large. Thus, the result of these "frozen in" excess quantities is a lower measured density at finite times and a slow increase in density over time as the material physically ages.

These explanations are consistent with the behavior we see in our resins. The maximum in density is found in resins which are near the gel point where the network has not yet severely restricted the packing of the chains, and a minimum amount of cooling has occurred in the glassy state. Fully cured resins have lower density than any resin beyond the gel point due to the severe restrictions on chain packing imposed by the tightly crosslinked networks, and because the maximum amount of cooling has occurred in the glassy state.

True stress–strain response

Compression testing is widely used to characterize the true material response of polymers subjected to large deformations. Others have shown that the initial stages of deformation are associated with the process history of the glass and large deformations are associated with the crosslinked network. The combination of deformation mechanisms activated in each region of the true stress versus true strain curves allows one to extract information about the state of physical ageing and network formation exhibited by the resins.

Figure 3 is a typical epoxy stress-strain curve that highlights some of the attributes of the experimental data discussed below. The true stress (σ_t) is plotted on the y-axis. The x-axis can be divided into the low strain regime, where we are interested in the true strain (ε_t) response, and the large strain regime where the neoHookian strain $-(\lambda^2-1/\lambda)$ is a better measure of the network response. λ is the compression ratio, measured as the current length (l) divided by the original length (l_0). The compressive modulus (E) is measured as the slope of the $\sigma_t-\varepsilon_t$ curve in the initial linear elastic regime. The yield stress (σ_y) is taken as the local maximum in the $\sigma_t-\varepsilon_t$ curve where large-scale plastic deformation begins. The rejuvenated stress (σ_r) is the local minimum in the $\sigma_t-\varepsilon_t$ curve after yield. The postyield stress drop is due to a combination of network packing and network connectivity effects. It can be parameterized as $K_y = \sigma_y/\sigma_r$ for the calculation of necking and shear banding stability. Beyond the local stress minimum after yield, the stress increases again with further deformation. At this point, it is more convenient to use a neoHookian strain term, instead of true strain, because the slope of the σ_t versus $-(\lambda^2-1/\lambda)$ curve is the strain hardening modulus (G_R), which is used to calculate network connectivity in terms of the molecular weight between crosslinks (M_c). Each of these regions will be discussed in subsequent sections.

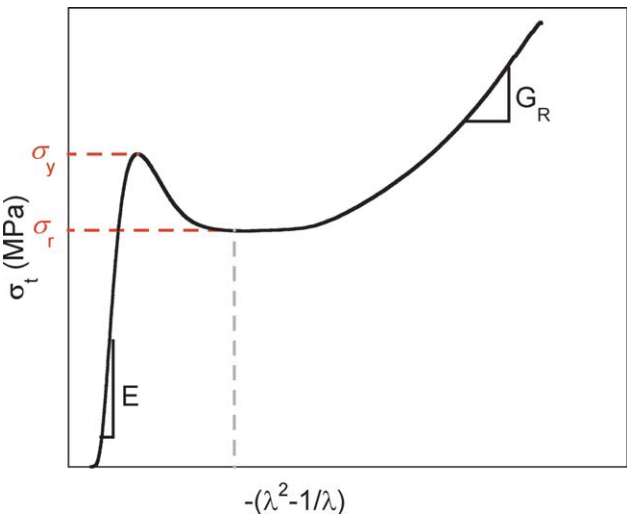

Figure 3 Typical true stress versus neo-Hookian strain compression curve. Dark dashed lines represent yield stress and rejuvenated stress. Light dashed line divides low and high strain regions. [Color figure can be viewed in the online issue, which is available at www.interscience.wiley.com.]

The true stress-neoHookian strain curves of resins cured using isothermal and ramp cure conditions are displayed in Figure 4(a,b), respectively. For small strains $-(\lambda^2-1/\lambda) \approx \varepsilon_t-1$, which amounts to shifting the origin to zero in the small strain regime. The series of isothermal and ramp-cured resins clearly show qualitative differences between resins with different T_g's within each series. For comparison, the curves are labeled with the T_g of the resins. At low T_g (e.g., low conversion) there is a pronounced stress maximum followed by a significant drop in stress. The magnitude of this stress maximum decreases and flattens out as T_g increases. In addition, the initial slope of the deformation curves decreases as a function of T_g, whereas the slope at high strains increases as T_g increases. These progressions in the slopes of the curves are caused by changes in network packing and network connectivity, respectively. The characteristics of each region of the curves will be discussed in detail in the sections that follow.

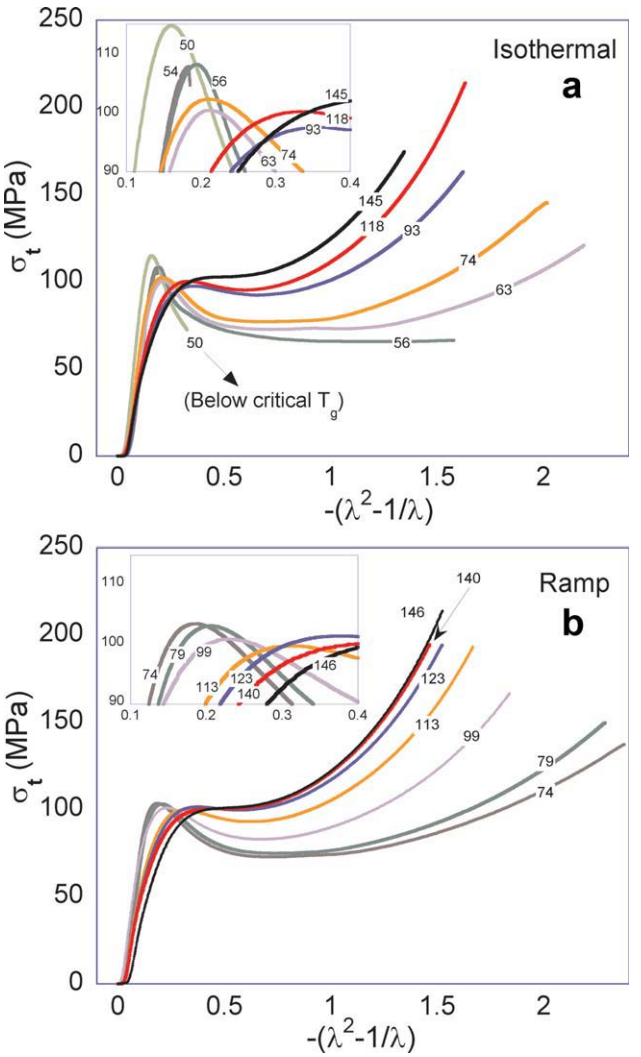

Figure 4 True stress vs neo-Hookian strain for (a) isothermally cured resins and (b) ramp cured resins. Curves are labeled with their *Tg*'s. Inset is an expansion of the yield region. [Color figure can be viewed in the online issue, which is available at www.interscience.wiley.com.]

Modulus

The modulus of polymers in the glassy state is sensitive to molecular packing,[38] and it typically correlates well with density. Just as Figure 1(b) demonstrates a decrease in density with T_g, Figure 5(a) highlights the decrease in modulus with T_g for resins in both the isotheral and the ramp cure series. The decrease in modulus as T_g increases has been previously reported in work on other resin systems.[29,39,40] In this system, resins with T_g values well below 145°C have significant levels of unreacted amine and epoxide groups. These groups are thought to be able to pack more efficiently than network chains because they have more conformational freedom than the chains that are fully incorporated into the network (i.e., fully reacted segments).[40] A similar argument can be made in terms of physical ageing. Modulus increases as a result of physical ageing where decreased free volume and longer relaxation times increase the apparent stiffness of materials.[2] From Figure 5(a), it is clear that modulus decreases as T_g increases. When subjected to cure conditions that achieve the maximum T_g, either initially or as a postcure step, all samples have approximately the same modulus regardless of the initial cure conditions. Therefore, cure path does not appear to affect the modulus of fully cured resins. However, physical ageing appears to be highly correlated with T_g in the partially cured resins.

Yield

Yielding is a thermally activated stress-induced material response.[41] It is the manifestation of macroscopic plastic flow in polymer systems. When inter- and intramolecular forces are no longer sufficient to elastically store additional mechanical energy localized shear bands begin to grow through the volume of the material.[9] In Figure 5(b), we observe higher yield stresses in resins with low T_g's.

Many authors have shown that yield stress increases when a polymer is physically aged.[1–3,9,42] However, yield stress levels off around 100 MPa for resins with T_g greater than 60°C in the isothermal and ramp cure series. It is important to note that resins in both series with T_gs below 50°C fail to achieve yield. Below this low T_g threshold, axial cracks propagate through the samples before a macroscopic yield condition is satisfied. Other authors have also commented on the difficulty in machining and testing epoxy resins with low conversions because they are extremely brittle and weak.[32] Axial cracking under uniaxial compression has been observed in brittle inorganic materials.[43] This fracture is thought to result from an inhomogeneous stress distribution at the platen-sample interfaces and the concurrent inability of the materials to sustain even relatively low levels of localized shear. As mentioned in the introduction, the yield point is considered to be the point at which shear bands begin to propagate through the whole compression bullet. This argument suggests lubrication and absolutely parallel platens and sample ends could help to alleviate this issue. However, perfect lubrication and alignment cannot overcome the susceptibility of inherently flawed networks, such as highly undercured epoxies, to brittle fracture. Therefore, there appears to be a threshold of network formation, in the vicinity of the gel point, before which these epoxy resins cannot be evaluated in the large strain regime using this technique. Below, we consider how the interplay between yield and postyield behavior can be used to predict the conditions necessary to stabilize shear deformation.

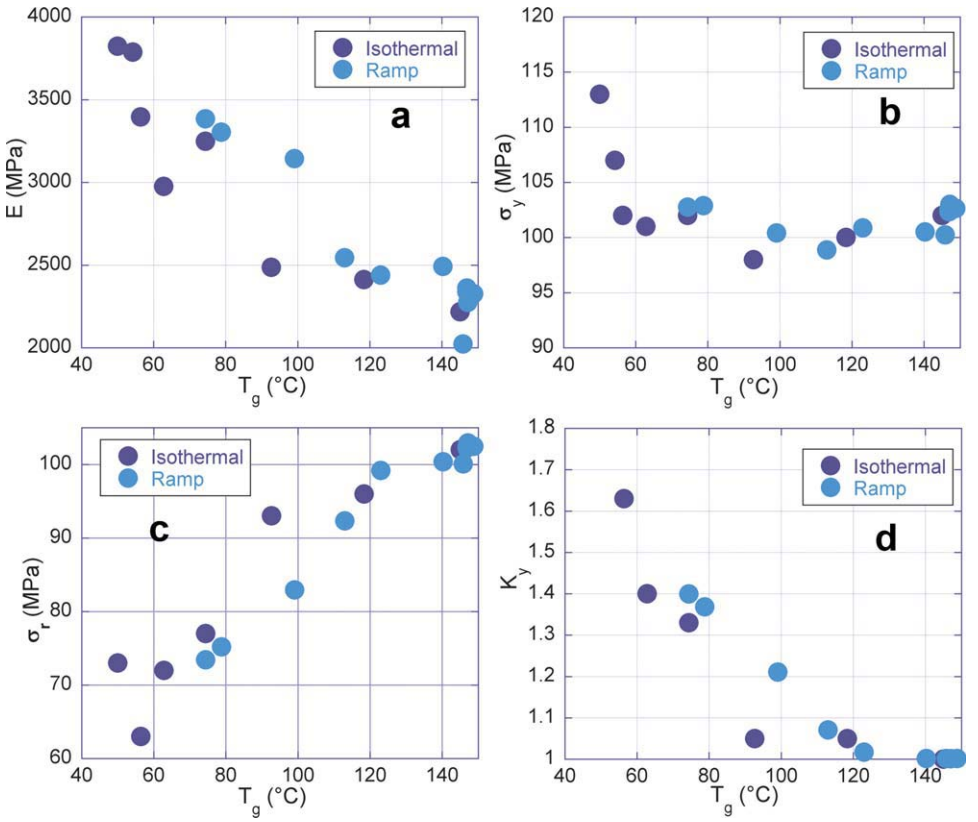

Figure 5 Physical and mechanical properties as functions of *Tg*. (a) modulus, (b) compressive yield stress, (c) rejuvenated stress, and (d) strain localization constant. [Color figure can be viewed in the online issue, which is available at www.interscience.wiley.com.]

Postyield response

The local minimum in the stress after yield is referred to as the rejuvenated stress (σ_r) for its relationship with the erasure of physical ageing. Haward and Cross and several subsequent authors found that subjecting polymers to mechanical deformation beyond yield can remove some of the effects of physical ageing e.g., rejuvenating the material.[1,4,9,44,45] As a dramatic example, Govaert et al. were able to demonstrate affine deformation of polystyrene in tension by mechanical preconditioning.[46] Another common method for removing physical ageing is to anneal a material above T_g, then quench it to a temperature well below T_g where physical ageing is very slow. Although quite useful with fully cured resins, thermal rejuvenation is not practical with the current reactive partially cured resins since heating above T_g will advance the curing reaction. Other less reactive systems, such as DGEBA cured with diaminodiphenylsulfone (DDS), may have some processing window above T_g where partially cured resins can be thermally equilibrated for a short time without significantly advancing the cure.[11] It has also been demonstrated that mechanical rejuvenation is not equivalent to thermal rejuvenation.[4,47] As such, the thermomechanical history of a sample can strongly influence deformation behavior.

Thermomechanical history is relevant to the current study because partially cured resins with different thermal histories are compared. If mechanical rejuvenation takes place in these materials the postyield response should only depend on the viscous flow properties of the networks rather than any thermomechanical history.[9,48] Figure 5(b) demonstrates the complex relationship between yield stress and T_g, and supports the argument that yield is sensitive to molecular packing and physical ageing. In contrast, Figure 5(c) shows that the rejuvenated stress appears to be linearly proportional to T_g. The proportionality between rejuvenated stress and T_g, and the fact that both sets of data points fall on the same curve, suggests the rejuvenated stress is insensitive to any molecular packing or physical ageing that may take place during the curing process. Therefore, the long-range network connectivity is the dominant factor affecting the rejuvenated stress.

None of the resins treated here have been subjected to mechanical or thermal pretreatments besides the thermal treatment used to cure them (see Methods). However, the stress–strain curves of the partially cured resins depicted in Figure 4(a,b)

clearly show rejuvenated stresses that are lower than the yield stress. Only the resins taken to full cure at 165°C have a negligible decrease in stress after yield, which indicates the absence of physical ageing. The difference between the yield stress and the rejuvenated stress is often referred to as strain softening, which is a manifestation of strain localization associated with physical ageing. Beyond the yield point localized deformation takes place in shear bands. The macroscopically measured stress continues to decrease as the shear bands expand to incorporate more material. When the shear bands have expanded to include all the material in a compression bullet, the local stress minimum or the rejuvenated stress is obtained. Further deformation is affine in nature, similar to deforming an elastomer above T_g. Others have argued that deforming a material to the yield point is the mechanical analog of lowering the T_g of a material to the test temperature.[41] In any case, the true stress-true strain response, where the rejuvenated stress is measured and at higher strains, is highly dependent on network connectivity and relatively less dependent on molecular packing.

To compare the cure dependence of different resin systems it would be convenient to parameterize the effect of physical ageing in the transition zone between processing dependent and network connectivity dependent properties. The yield stress offers information about how physical ageing and the local chain packing environment affects a material's resistance to flow, whereas the rejuvenated stress offers insight into how the network connectivity affects resistance to flow. Normalizing the yield stress by the rejuvenated stress gives a dimensionless strain localization parameter ($K_y = \sigma_y/\sigma_r$) that can be applied to various resin systems, including thermoplastics.[3] K_y quantifies the excess stress required to initiate large-scale plastic deformation in a material (i.e., yield stress) relative to the stress required to continue deforming the material beyond yield (i.e., rejuvenated stress). Numerous authors have demonstrated the strain-rate and temperature dependence of yield stress and the rejuvenated stress, so K_y is necessarily dependent on those variables as well.[3,6,34,49–54]

Figure 5(d) is a plot of K_y versus T_g, where we see an inverse proportionality between K_y and T_g. K_y approaches one as the resins approach the maximum T_g. Therefore, there is an insignificant amount of strain localization that occurs in the deformation of fully cured resins. This lack of strain localization implies that physical ageing is removed as network formation proceeds.

Strain hardening

Much of what we know about the strain-hardening responses of polymer networks appears in the literature on thermoplastics and rubbers. Constitutive relationships have been developed to describe large-strain deformation where molecular entanglements form the basis of network structures.[3,5,34,52,54–56] One theme that is derived from the rubber elasticity approach of these constitutive relationships is the idea that networks display an entropic hardening response at high strains. This nonlinear behavior can be captured by using a nonlinear measure of strain such as the neoHookian strain. Here, the strain-hardening modulus (G_R) is the slope of the true stress (σ_T) versus neoHookian strain curve as given by eq. (3).

$$G_R = -\frac{\partial \sigma_T}{\partial\left(\lambda^2 - 1/\lambda\right)} \tag{3}$$

where λ is the extension ratio. The molecular weight between entanglements (M_e) is calculated from eq. (4), which was originally developed to describe transient molecular entanglement networks in thermoplastics.[52]

$$M_e = \frac{\varphi \rho RT}{G_R} \tag{4}$$

where ρ is the mass density, R is the ideal gas constant, T is the absolute temperature, and φ is a constant related to crosslink mobility and is assumed to be equal to 1 for immobile crosslinks.[33,57] Equation (4) can be applied to thermosets with high crosslink densities by assuming crosslinks and chain entanglements are analogous such that $M_c = M_e$, where M_c is the molecular weight between crosslinks.

Equations (3) and (4) provide a way to interpret the strain-hardening responses of networks in terms of network architecture. Similar to the effect seen in the rejuvenated stress, differences in network connectivity are assumed to be the dominant factor affecting the mechanical response in the strain-hardening regime.[50,51,58,59] The strain hardening modulus (G_R) is the value from eq. (3) at 90% of the ultimate true strain. Using the value of G_R calculated at a strain equal to 90% of the ultimate true strain samples G_R at a location that is equivalent for each resin. In the case of perfect adherence to the constitutive model, the true stress would increase linearly with respect to neoHookian strain in the strain hardening regime, whereas we see a slight increase in slope as strain increases in this regime. Several authors have commented that the true stress versus neoHookian strain curve increases faster than linearly due to finite extensibility considerations and the non-Gaussian deformation behavior of tightly crosslinked networks in the glassy state.[51,60] While more accurate stress–strain measures incorporating inverse Langevin and other strain functions have been

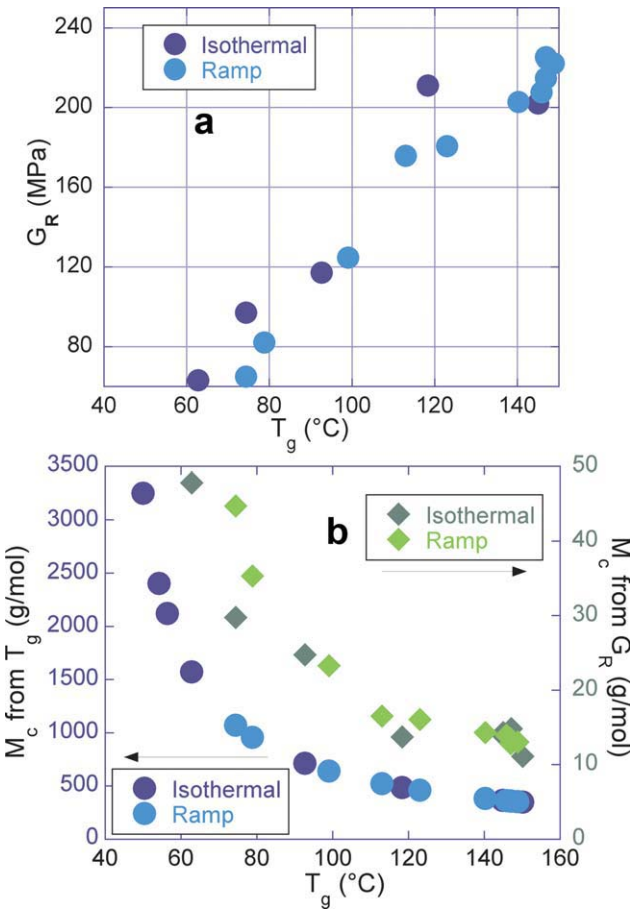

Figure 6 (a) Strain hardening modulus as a function of *Tg*. (b) M_c as a function of T_g. Left *y*-axis applies to M_c values calculated from eq. (6) (i.e., from *Tg*). Right y-axis applies to M_c calculated from eq. (4) (i.e., from *GR*). [Color figure can be viewed in the online issue, which is available at www.interscience.wiley.com.]

proposed,[52,54,55] the current method is sufficient to highlight the trends found herein.

Figure 6(a) demonstrates the proportionality between G_R and T_g. According to eq. (3), G_R is inversely proportional to M_c. Since the density and test temperature are essentially constant between samples in both series of resins in Figure 6(a), G_R is the main factor affecting the calculated value of M_c.

M_c can also be calculated from the molecular weights of the epoxy and amine monomers [eq. (5)].

$$M_c = 2*(M_p + M_a), \tag{5}$$

where M_p is the epoxide equivalent weight ($\sim$ 175 g/mol for DGEBA), M_a is the amine equivalent weight (15 g/mol for EDA), and all crosslinks are assumed to be tetrafunctional.[61] For the ideal case of a stoichiometric EDA-DGEBA resin taken to full cure, M_c is equal to 380g/mol. The value of M_c calculated from G_R is an order of magnitude smaller than the value calculated from stoichiometry. Previous work by other authors has found a similar discrepancy between calculations based on stoichiometry and sub-T_g mechanical characterizations of M_c.[18,61] The rubber elasticity-based theory used to calculate M_c is expected to deviate from ideality here due to the non-Gaussian conformations of chains in highly crosslinked glassy networks, steric interactions, and trapped entanglements.[22,34,57] However, we have demonstrated that strain-hardening modulus increases as the cure state advances so the correlation between the large strain mechanical response and network connectivity proves to be qualitatively correct despite a quantitative discrepancy.

To compare the M_c calculated from the mechanical response with another method that is valid over a wide range of cure conditions, a semiempirical calculation of M_c based on T_g can be used [eq. (6)].

$$M_c = \frac{\zeta}{T_g - T_{g\infty}} \tag{6}$$

where ζ is a crosslink mobility parameter taken to be equal to 39 kg/Kmol, and $T_{g\infty} = 311$ K is the T_g of the linear epoxy/amine analog of infinite molecular weight (i.e., difunctional amine cured epoxy resin).[62,63] Figure 6(b) shows that the trends between M_c and T_g from the two methods are in excellent qualitative agreement, however, the M_c values differ by a factor of approximately 100. Previous work in our group has shown that this factor decreases as the test temperature approaches and exceeds the T_g of epoxy networks with stoichiometrically controlled M_c[49]. Unfortunately, the partially cured resins treated here cannot be tested at elevated temperatures because curing proceeds rapidly above T_g.

Strain localization

The decrease in stress after yielding, mentioned earlier, is the macroscopic manifestation of localized deformation, which is initiated by the response of microscopic defects to loading. Localized regions of flowing material behave in a softer manner than the surrounding undeformed material. However, the softening is balanced by strain hardening. Flow-induced orientation causes deformed material to become stiffer. Thus the deformation zones expand to include more material. The balance of the softening and hardening responses greatly affects material responses, as Govaert and coworkers demonstrated in their illustrative work on polystyrene and polycarbonate.[3] In compression, polystyrene typically has a decrease in stress after yield ($K_y = 1.6$) and a low strain hardening modulus. Polycarbonate also

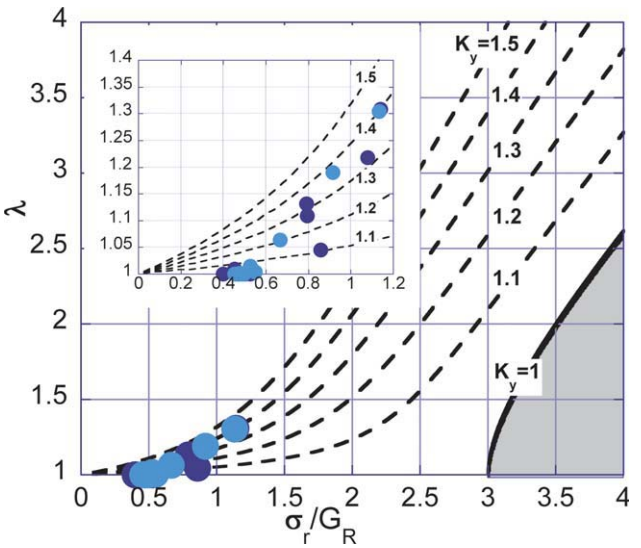

Figure 7 Neck stability contour map. Dark circles are for Isothermal samples. Light circles are for Ramp cure samples. Values of λ are calculated by solving eq. (7). Inset expands the region containing experimental data. *Ky* equilibrium isolines are labeled with *Ky* values, and *Ky*, σ*r*, and *GR* are measured from compression tests. [Color figure can be viewed in the online issue, which is available at www.interscience.wiley.com.]

has a significant drop in stress after yield ($K_y = 1.4$), but the ratio of its strain hardening modulus to its rejuvenated stress is much higher than that of polystyrene. The result is that strain is much more localized in polystyrene than in polycarbonate, which qualitatively changes which deformation mechanisms are activated.

An early treatment of strain localization was Haward's necking stability analysis.[56] He considered the relationship between rejuvenated stress and strain-hardening modulus in tension. Equation (7) is the equation presented by Haward[56] and adjusted by van Melick et al.,[3] which predicts the stability of a neck.

$$\frac{\sigma_r}{G_R} = \frac{\lambda^2 - 1/\lambda}{K_y\lambda - 1} \tag{7}$$

where σ_r is the rejuvenated stress, G_R is the strain-hardening modulus, λ is the extension ratio of material in the neck, and K_y is the strain localization constant, which were all defined in previous sections. Figure 7 is a contour map which predicts qualitative deformation behavior of isothermal and ramp cured epoxies in tension (after van Melick et al.[3] and Haward[56]). The data points on the graph represent the intersection of the equilibrium (K_y) lines and the values of σ_r/G_R determined from compression tests according to eq. (7). The values of λ corresponding to the data points are the predicted extension ratios of material in a neck necessary to stabilize the neck. As K_y increases the extension ratio necessary to stabilize a neck increases. Therefore, physical ageing, which increases K_y, imposes a more severe orientation requirement on a material. In the absence of physical ageing (i.e., K_y equal to 1) necking behavior depends only on σ_r/G_R. In that case, if $\sigma_r/G_R < 3$ deformation is intrinsically affine, whereas if $\sigma_r/G_R > 3$ the material will form a stable neck. Most polymers in the glassy state have a value of $K_y > 1$, and this strain localization promotes the formation of a neck in tension. The greater K_y is, the greater the orientation in the neck. Certain thermomechanical histories will either promote or inhibit necking. For example, mechanically deforming PVC, polycarbonate, or polystyrene in the glassy state has been shown to temporarily prevent necking.[1,3,55,56] Conversely, physically ageing polymers by annealing them for long times at temperatures below T_g has been shown to increase K_y, and thus promote strain localization in the form of a more highly oriented neck.[64]

The epoxy resins treated here are glassy thermosets with values of K_y between 1 and 1.5, and σ_r/G_R less than 1.5. The fully cured resins have K_y equal to 1. Therefore, the plot predicts they will undergo affine deformation in tension. Resins with T_g less than 145°C have K_y values ranging up to about 1.6 [Fig. 5(d)]. Therefore, the plot predicts they should form stable necks in tension at relatively low extension ratios. In practice, stable necking is not observed. The maximum extension ratio observed in tension with these resins is $\lambda \approx 1.05$. Strain localization activates mode I failure at very low macroscopic strains when these resins are loaded in tension. Therefore, they tend to fail before they can achieve extension ratios where necking might be stabilized. Other workers have demonstrated that tensile testing conducted at elevated temperatures approaching T_g allows crosslinked epoxies to be deformed beyond the yield point.[16]

Shear band stability

It is well established that shear band formation and necking are phenomena that arise in glassy polymers from a material instability (strain softening followed by subsequent strain hardening) after the polymer yields. In the case of neck formation, the material instability is compounded with a geometric instability. As mentioned earlier, loading in compression suppresses mode I failure, allowing otherwise brittle materials to be taken to higher strains where yield and postyield behavior can be characterized. However, loading in compression also eliminates the geometric instability that causes necking. Therefore, the predominant deformation mechanism in compression is shear banding.

Haward and others[3,56] have established stability conditions for neck formation based on establishing equilibrium across the necked and unnecked regions, respectively. Their result provides conditions for neck formation in terms of the extension ratio (λ) and other characteristics of the post yield response of the polymer [see eq. (7)]. In what follows, we extend the concept by applying the same approach for the stability of a shear band.

For the case of a shear band, the force balance between the applied far-field shear stress and the true shear stress in the shear band is given by eq. (8).

$$\tau_o A_o = \tau A \tag{8}$$

where A_o is the initial cross-sectional area, and A is the instantaneous cross-sectional area. From rubber elasticity, eq. (9) describes a generalized strain energy function (F), where G is the strain-hardening modulus and λ_1, λ_2, and λ_3 are the extension ratios.

$$F = 1/2 G(\lambda_1^2 + \lambda_2^2 + \lambda_3^2 - 3) \tag{9}$$

$$\lambda_1 = \lambda, \lambda_2 = 1, \lambda_3 = 1/\lambda \tag{10}$$

In a shear band we define the strain as occurring at constant volume ($\lambda_1\lambda_2\lambda_3 = 1$) in a plane according to eq. (10). Applying these constraints to equation 9, and combining terms we get our strain energy function [eq. (11)].

$$F = 1/2 G\left(\lambda - 1/\lambda\right)^2 \tag{11}$$

The engineering stress (σ_e) is given by eq. (12).

$$\sigma_e = \frac{\partial F}{\partial \lambda} \tag{12}$$

However, we are interested in the shear stress (τ).

$$\tau = \frac{\partial F}{\partial \gamma} \tag{13}$$

where

$$\gamma = \left(\lambda - 1/\lambda\right) \tag{14}$$

such that

$$\tau = \frac{\partial}{\partial \gamma}\left(1/2 G\gamma^2\right) \tag{15}$$

Thus, the shear stress (τ) is given by eq. (16).

$$\tau = G\gamma = G\left(\lambda - 1/\lambda\right) \tag{16}$$

Following the approach of Haward [56]

$$\tau_y = \tau_r + G\left(\lambda - 1/\lambda\right) \tag{17}$$

where τ_y is the shear yield stress and τ_r is the rejuvenated shear stress. We can relate τ_y and τ_r through the physical ageing constant (K_y).

$$\tau_y = K_y \tau_r \tag{18}$$

By rearranging Equation M and substituting for τ_y, we get

$$\frac{\tau_r}{G} = \frac{\left(\lambda - 1/\lambda\right)}{K_y - 1} \tag{19}$$

Following a von Mises yield condition, the octahedral shear stress (τ^{oct}) is calculated according to eq. (20) and we can describe the shear stress in the rejuvenated regime in terms of the rejuvenated stress [eq. (21)].

$$\tau^{oct} \equiv 1/3\sqrt{(\sigma_1 - \sigma_2)^2 + (\sigma_2 - \sigma_3)^2 + (\sigma_3 - \sigma_1)^2} \tag{20}$$

$$\tau^{oct} = \sqrt{2}/3 \sigma_r = \tau_r \tag{21}$$

Substituting for τ_r in eq. (19) we obtain eq. (22), the shear band stability equation.

$$\sqrt{2}/3 \frac{\sigma_r}{G} = \frac{\left(\lambda - 1/\lambda\right)}{K_y - 1} \tag{22}$$

The level of orientation required to stabilize shear bands in a given network is lower than that required for necking stability. Whereas the epoxy resins treated here are incapable of forming necks at the test temperature and strain rate used, the less stringent critical extension ratio requirements for shear banding could allow some resins to stabilize shear bands.

To test the shear banding theory, samples were machined into notched rectangular compression specimens and tested in compression along the long axis of the specimens as depicted in Figure 8(a). To calculate the local shear strain a series of calibration lines were scratched into the surface of each sample perpendicular to the plane of shear. The local shear strain is calculated by dividing the displacement of each line in the direction of shear by the breadth of the sheared region according to eq. (23),

$$\gamma_{12} = \frac{u_{12}}{x_2} \tag{23}$$

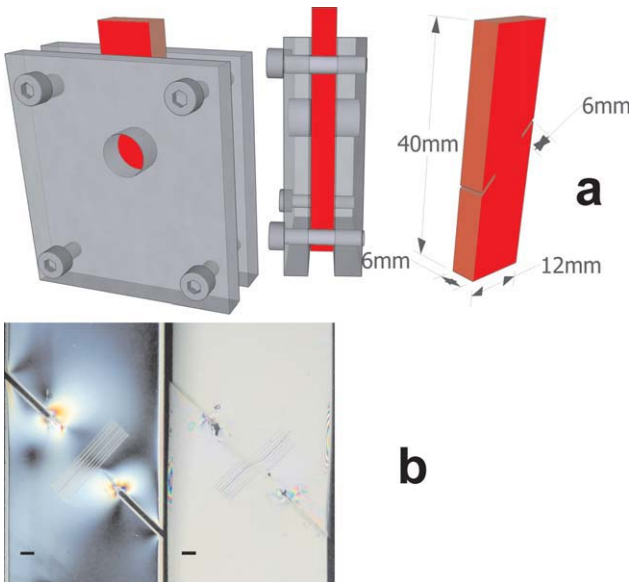

Figure 8 (a) Shear band support fixture and sample. (b) Shear sample before (left) and after (right) testing. Scale bar is 1 mm. [Color figure can be viewed in the online issue, which is available at www.interscience.wiley.com.]

where γ_{12} is the shear strain, u_{12} is the deformation along the plane of shear, and x_2 is the width of the sheared region. Figure 8(b) shows the plastically deformed regions of a shear sample before and after loading as seen under circularly polarized light. Resins fabricated with various cure conditions were tested to determine the differences in shearing characteristics as a function of T_g. Highly undercured resins with T_g less than 60°C were unable to achieve yield in shear. Axial cracking dominated the deformation beyond the initial elastic deformation with no formation of shear bands. Resins with T_g greater than 80°C were able to achieve measurable shear strains along a shear band between the precracked notches as observed in Figure 8(b).

The resins that did not achieve yield are also unable to support the orientation required to stabilize shear bands. According to the trends of both σ_y and G_R versus T_g, the resins which were unable to sustain plastic flow, even in compression, should have high yield stresses and very low-strain hardening moduli. Therefore, strain localization should be quite severe in these resins, leading to fracture at low deformation, which we observe in compression testing. There appears to be a threshold of network formation necessary to support macroscopic nonlinear deformation. In this work, the threshold appears to be a T_g of approximately 50°C, which corresponds to a conversion of (0.6 (i.e., the gel point)).

Figure 9 is a map of the shear band stability calculated from eq. (22). Similar to the necking stability map in Figure 7, the data points in Figure 9 represent the intersection of the equilibrium (K_y) lines and the values of σ_r/G_R determined from compression tests according to eq. (22). The values of λ corresponding to the data points are the critical extension ratios of material in a shear band necessary to stabilize the shear band. As K_y increases, the extension ratio necessary to stabilize a shear band increases, although less severely than for necking stability. In the absence of physical ageing, which increases K_y, imposes a more severe orientation requirement on material in a shear band. In the limit of number of physical ageing (i.e., K_y equal to 1) the model predicts λ in the shear band to be equal to 1. This implies that rejuvenated polymers and crosslinked polymers above T_g should not undergo shear banding. Therefore, affine deformation is predicted in the case where K_y is equal to 1.

Figure 9 shows that the measured values of λ from the shear test are higher than the predicted critical values calculated from compression data using eq. (22). This discrepancy suggests that material in the shear bands continues to orient beyond the critical extension ratio as deformation proceeds. One possible explanation for the excessive orientation behavior is local viscous heating caused by the flow. Other workers have shown that σ_r decreases as temperature increases.[3,34,49,55,59,65–67] The localized heating would increase the critical level of orientation of material in the shear band due to decreases in yield and rejuvenated stresses at higher temperatures. However, material outside of the shear band would not be heated so it would still require the higher stresses associated with cooler temperatures

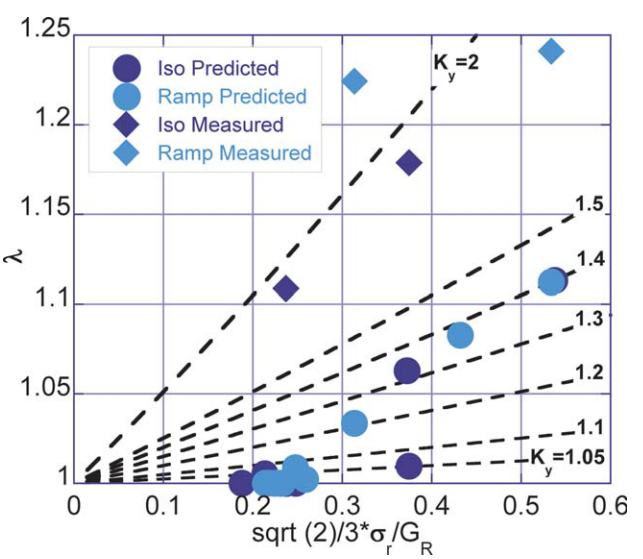

Figure 9 Shear band stability map. Dark circles are for Isothermal samples. Light circles are for Ramp cure samples. Values of λ are predicted by solving eq. (22). *Ky* equilibrium isolines are labeled with *Ky* values, and *Ky*, σ*r*, and *GR* are measured from compression tests. [Color figure can be viewed in the online issue, which is available at www.interscience.wiley.com.]

before being incorporated into the shear band. This rationalization is also dependent on strain rate and test temperature. Although local heating is a plausible explanation for the observed behavior, more work is needed to rigorously determine the deviations from the predicted behavior.

CONCLUSIONS

This study analyzes network formation of two series of partially cured stoichiometric epoxy-amine resins using thermal, mechanical, and physical probes. By systematically varying the cure states of the resins using an isothermal and a ramp cure condition we were able to map the mechanical responses of the resins at various stages of network formation. T_g was used as a metric of network formation due to its sensitivity to changes in network connectivity, particularly at high conversion. The physical and mechanical properties that are sensitive to molecular packing, such as density, compressive modulus, and yield stress were shown to be highly dependent on T_g as well. Qualitative changes in the density and yield stress were observed in the vicinity the gel point. The trends in the deformation behavior demonstrated an inverse relationship between characteristics of physical ageing and network formation in terms of mechanical properties. The decrease in segmental mobility associated with physical ageing was attributed to the enhanced ability of unreacted amine and epoxide groups to pack within the network. Taking resins to full cure by either an initial high temperature cure or a high temperature postcure was shown to remove any artifacts of physical ageing regardless of the initial cure state. High temperature curing also led to a decrease in room temperature density, consistent with the idea that the topologically constrained network is locked into a low density configuration when it is cooled in the glassy state. The result of advancing the cure state of a resin is the inhibition of physical ageing as measured by decreases in density, modulus, yield stress, and the strain localization constant.

The large-strain responses of the networks in the postyield regime were found to have little dependence on cure path, whereas they showed strong dependences on network connectivity. The rejuvenated stress was found to be highly correlated with T_g, and insensitive to the cure path. The strain-hardening modulus increased linearly with T_g. The trends between M_c and T_g, where M_c was calculated using a mechanical and a thermal method, respectively, were in excellent qualitative agreement with each other. However, the mechanical characterization underestimates M_c by a factor of approximately 100. This quantitative difference between M_c values is associated with the mechanical characterization of densely crosslinked epoxies in the glassy state.

The data from this work were also applied to two analyses of deformation instabilities. The resins were predicted to be able to stabilize necking in tensile tests, however mode I failure occurred before necking could be observed. When we applied our results to a shear banding stability model developed by our group, we found the resins were able to achieve sufficient extension ratios along a shear band to allow propagation of shear bands through the samples. In both necking and shear banding, analyses, decreases in the degree of strain localization were associated with increases in network formation in the epoxy resins.

The authors are grateful for the work of James Gorman as part of the Research Experience for Teachers program.

References

1. Cross, A.; Haward, R. N. Polymer 1978, 19, 677.
2. Struik, L. C. E. Physical Ageing in Amorphous Polymers and Other Materials; Elsevier: Amsterdam, 1978.
3. van Melick, H. G. H.; Govaert, L. E.; Meijer, H. E. H. Polymer 2003, 44, 3579.
4. McKenna, G. B. J Phys: Condens Matter 2003, 15, 737.
5. Klompen, E. T. J.; Engels, T. A. P.; Govaert, L. E.; Meijer, H. E. H. Macromolecules 2005, 38, 6997.
6. Ellis, B. Chemistry and Technology of Epoxy Resins; Chapman and Hall: New York, 1993.
7. Lee, A.; McKenna, G. B. Polymer 1988, 29, 1812.
8. Wang, X.; Gillham, John K. J Appl Polym Sci 1993, 47, 447.
9. G'Sell, C.; McKenna, G. B. Polymer 1992, 33, 2103.
10. Detwiler, A.; Lesser, A. J. Network Formation in Glassy Thermosets. ANTEC: Milwaukee, Massachusetts, 2008.
11. White, S. R.; Mather, P. T.; Smith, M. J. Polym Eng Sci 2002, 42, 51.
12. Rana, D.; Sauvant, V.; Halary, J. L. J Mater Sci 2002, 37, 5267.
13. Wang, X.; Gillham, J. K. J Appl Polym Sci 1993, 47, 425.
14. Montserrat, S. J Appl Polym Sci 1992, 44, 545.
15. Cook, W. D.; Scott, T. F.; Quay-Thevenon, S.; Forsythe, J. S. J Appl Polym Sci 2004, 93, 1348.
16. Tcharkhtchi, A.; Trotignon, J. P.; Verdu, J. Macromol Sympos 1999, 147, 221.
17. Madsen, P. A.; Foister, R. T. J Appl Polym Sci 1989, 37, 1931.
18. Calzia, K. J.; Lesser, A. J. ANTEC 2006.
19. Wang, X.; Gillham, J. K. J Appl Polym Sci 1992, 45, 2127.
20. Jordan, C.; Jocelyne, G.; Jean-Pierre, P. J Appl Polym Sci 1992, 46, 859.
21. Verchere, D.; Sautereau, H.; Pascault, J. P.; Riccardi, C. C.; Moschiar, S. M.; Williams, R. J. J. Macromolecules 1990, 23, 725.
22. Charlesworth, J. M. Polym Eng Sci 1988, 28, 221.
23. Matejka, L. Macromolecules 2000, 33, 3611.
24. Flory, P. J. Principles of Polymer Chemistry; Cornell University Press: Ithica, 1953.
25. Flory, P. J. J Am Chem Soc 1941, 63, 3083.
26. Swier, S.; Van Assche, G.; Van Mele, B. J Appl Polym Sci 2004, 91, 2798.
27. Wang, X.; Gillham, J. K. J Appl Polym Sci 1991, 43, 2267.
28. Pang, K. P.; Gillham, J. K. J Appl Polym Sci 1989, 37, 1969.
29. Ellis, B.; Found, M. S.; Bell, J. R. J Appl Polym Sci 1996, 59, 1493.

30. Brady, R. F. J Macromol Sci Rev Macromol Chem Phys 1992, C32, 135.
31. Shimbo, M.; Ochi, M.; Shigeta, Y. J Appl Polym Sci 1981, 26, 2265.
32. Jordan, C.; Galy, J.; Pascault, J.-P. J Appl Polym Sci 1992, 46, 859.
33. Varley, R. J.; Hodgkin, J. H.; Simon, G. P. J Appl Polym Sci 2000, 77, 237.
34. Ferry, J. D. Viscoelastic Properties of Polymers; Wiley: New York, 1980.
35. Venditti, R. A.; Gillham, J. K.; Jean, Y. C.; Lou, Y. J Appl Polym Sci 1995, 56, 1207.
36. Kovacs, A. J.; Stratton, R. A.; Ferry, J. D. J Phys Chem 1963, 67, 152.
37. Johari, G. P. In Disorder Effects on Relaxational Processes; Richert, R.; Blumen, A., Eds.; Springer-Verlag: Berlin, 1994; pp 627–657.
38. Haward, R. N.; Young, R. J. The Physics of Glassy Polymers; Chapman and Hall: New York, 1997.
39. Halary, J. L. High Perform Polym 2000, 12, 141.
40. Enns, J. B.; Gillham, J. K. J Appl Polym Sci 1983, 28, 2831.
41. Robertson, R. E. J Chem Phys 1966, 44, 3950.
42. Golden, J. H.; Hammant, B. L.; Hazell, E. A. J Appl Polym Sci 1967, 11, 1571.
43. Vardoulakis, I.; Labuz, J. F.; Papamichos, E.; Tronvoll, J. Int J Solids Struct 1998, 35, 4313.
44. Oyanguren, P. A.; Vallo, C. I.; Frontini, P. M.; Williams, R. J. J. Polymer 1994, 35, 5279.
45. Tervoort, T. A.; Govaert, L. E. J Rheol 2000, 44, 1263.
46. Govaert, L. E.; van Melick, H. G. H.; Meijer, H. E. H. Polymer 2001, 42, 1271.
47. van Melick, H. G. H.; Govaert, L. E.; Raas, B.; Nauta, W. J.; Meijer, H. E. H. Polymer 2003, 44, 1171.
48. Oyanguren, P. A.; Vallo, C. I.; Frontini, P. M.; Williams, R. J. J. Polymer 1994, 35, 5279.
49. Calzia, K. J.; Lesser, A. J. Post-yield Deformation of Glassy Networks: Effects of Molecular Architecture. ANTEC: Charlotte, North Carolina, 2006.
50. Hoy, R. S.; Robbins, M. O. J Polym Sci Part B: Polym Phys 2006, 44, 3487.
51. Boyce, M. C.; Arruda, E. M. Rubber Chem Technol 2000, 73, 504.
52. Treloar, L. R. G. The Physics of Rubber Elasticity; Oxford University Press: Oxford, United Kingdom, 1975.
53. Wang, X. R.; Foltz, V. J. Polymer 2006, 47, 5090.
54. Boyce, M. C.; Arruda, E. M. Polym Eng Sci 1990, 30, 1288.
55. Tervoort, T. A.,Govaert, L. E. J Rheol 2000, 44, 1263.
56. Haward, R. N. Polymer 1987, 28, 1485.
57. Charlesworth, J. M. Polym Eng Sci 1988, 28, 230.
58. Haward, R. N. Y.,R. J. The Physics of Glassy Polymers; Chapman and Hall: New York, 1997.
59. van Melick, H. G. H.; Govaert, L. E.; Meijer, H. E. H. Polymer 2003, 44, 2493.
60. Haward, R. N.; Thackray, G. Proc R Soc London Ser A 1968, 302, 453.
61. Lesser, A. J.; Crawford, E. J Appl Polym Sci 1997, 66, 387.
62. Crawford, E. D. L.; Alan, J. J Polym Sci Part B: Polym Phys 1998, 36, 1371.
63. Crawford, E. D. L.; Alan, J. Polym Eng Sci 1999, 39, 385.
64. Klompen, E. T. J.; Engels, T. A. P.; Govaert, L. E.; Meijer, H. E. H. Macromolecules 2005, 38, 6997.
65. Arruda, E. M.; Boyce, M. C.; Jayachandran, R. Mech Mater 1995, 19, 193.
66. Boyce, M. C.; Arruda, E. M. Rubber Chem Technol 2000, 73, 504.
67. Kontou, E. J Appl Polym Sci 1996, 61, 2191.